Acta Cryst. (1951). **4**, 310

The Crystal Structure of Boracite

BY T. ITO, N. MORIMOTO AND R. SADANAGA

Mineralogical Institute, Science Department, University of Tokyo, Japan

(*Received* 2 *November* 1950)

The structures of high- and low-boracite have been analysed using powder and Weissenberg photographs (Mo $K\alpha$, $\lambda = 0{\cdot}71$ A., Cu $K\alpha$, $\lambda = 1{\cdot}54$ A.). The unit cells and space groups are:

	a (A.)	b (A.)	c (A.)	No. of molecules in the unit cell	Space group
High-boracite	12·1	— (at 300° C.)	—	8 ($ClMg_3B_7O_{13}$)	T_d^5–$F\bar{4}3c$
Low-boracite	8·54	8·54	12·07	4 ($ClMg_3B_7O_{13}$)	C_{2v}^5–Pca

The two structures are essentially the same, both containing the same boron–oxygen network and differing only in the positions of magnesium and chlorine atoms. The network may be described as a rigid aggregate of BO_4 tetrahedra and BO_3O pyramids which, sharing every oxygen corner, extend indefinitely throughout the structure. A new concept of the α–β inversion of boracite is suggested.

Boracite possesses peculiar properties which have attracted attention not only of crystallographers but also of physicists since the earliest days of crystallography. Of numerous investigations we may mention here particularly those of Mehmel (1934*a*, *b*), who determined the unit cells and space groups of the two modifications of boracite and tried to interpret the relationships between them. We describe below the results of our study of this classic example of mimetism carried out following the work of Mehmel and others (e.g. Beckenkampf, 1933, vol. 1, p. 104).

As material for study we have used a number of light-blue crystals from Stassfurt, Germany, which, with (110) well developed, measured several millimetres in diameter.

1. The structure of high-boracite*

(i) *Experimental*

Using a high-temperature camera of the type described by Cohn (1928), powder photographs (Cu $K\alpha$, $\lambda = 1{\cdot}54$ A.) were taken at 300° C. The exposure time varied from 2 to 4 hr.

(ii) *Unit cell and space group*

The cubic cell has $a = 12{\cdot}1$ A. There are eight molecules of $ClMg_3B_7O_{13}$ in the cell. On the basis of morphological and other observations, the space group has been determined to be T_d^5–$F\bar{4}3c$, with hkl reflexions present only when $h+k$, $k+l$ and $l+h$ are even and hhl reflexions only when h and l are even. These findings are in complete agreement with the previous ones (Mehmel, 1934*b*).

* Following the procedure of Sosman (1924) for silica, we designate as 'high-' and 'low-boracite' crystals above and below 265° C., the α–β inversion temperature.

(iii) *Analysis*

The presence of (531), (731) and other reflexions with h, k and l all odd suggests, due regard being paid to the structure amplitude for $F\bar{4}3c$, that atoms of one kind or another must be in $(h)x, y, z$ positions (*International Tables* (1935), p. 333). We, therefore, set aside 96 of the 104 oxygen atoms in the cell for the general positions. The 8 remaining oxygen and 8 chlorine atoms should, then, be either in $(a)0, 0, 0$ or $(b)\frac{1}{4}, \frac{1}{4}, \frac{1}{4}$ positions, each with 8 equivalent points. Next, we split the 56 boron atoms in the cell into two groups of 24 and 32 atoms. Whereas for the latter group there is no other appropriate position than $(e)x, x, x$, we have for the former two alternative positions, viz. $(c)0, \frac{1}{4}, \frac{1}{4}$ and $(d)\frac{1}{4}, 0, 0$. This applies also to 24 magnesium atoms contained in the unit cell. Hence, in assigning parameters to atoms, we have formally four different combinations of positions to consider. These, however, are identical in pairs, leaving only two:

	A	*B*
8 O	(*a*)	(*a*)
8 Cl	(*b*)	(*b*)
24 Mg	(*d*)	(*c*)
24 B	(*c*)	(*d*)
32 B	(*e*)	(*e*)
96 O	(*h*)	(*h*)

Whichever we choose of the two combinations, 32 boron atoms as well as 8 oxygen atoms lie on the trigonal rotation axes, around which 96 oxygen atoms in the general positions, grouped in threes, should be co-ordinated in a triangular form. Disregarding the presence of other atoms, we can conceive of these atoms making up an oxygen tetrahedron with a boron atom in the middle, or, more generally, a trigonal pyramid with oxygen atoms at the corners and a boron atom within or at the centre of its base.

We assumed the boron position and O–O distances of the pyramid appropriately, and rotated it about the trigonal axis until we obtained a structure which, together with chlorine, magnesium and other boron atoms at the fixed positions (*B*-combination), explained roughly the experimental data. The final positions of atoms, determined as usual by the trial-and-error method, are given in Table 1. We give in Table 2 the calculated F values and intensities compared with those derived from visual estimation on the photographs.

Table 1. *Atomic co-ordinates of high-boracite*

Atom	No. of equivalent points in the cell	x/a_1	y/a_2	z/a_3
O_I	8	0	0	0
O_{II}	96	0·021	0·098	0·180
Cl	8	0·250	0·250	0·250
Mg	24	0·250	0·250	0
B_I	24	0·250	0	0
B_{II}	32	0·085	0·085	0·085

Further, the two-dimensional Fourier method has been tried. Although experimental data are of necessity rather scanty in this higher-temperature range of boracite, the result of synthesis seems to support the structure arrived at.

(iv) *Description of structure*

The structure of high-boracite is illustrate in Fig. 1, projected on a cube face, and the corresponding Fourier projection is given in Fig. 2.

The structure is a three-dimensional boron–oxygen network interspersed with magnesium and chlorine atoms. For convenience of description, however, we may picture a group, B_5O_{12}, singled out arbitrarily from the structure. The B_5O_{12} group is a BO_4 tetrahedron with all the oxygen atoms at its corners each forming part of a BO_3 triangle (Fig. 3). All four BO_3 triangles are independent and related to each other only indirectly through the oxygen atoms of the central BO_4 tetrahedron. Further, the BO_3 group is not strictly planar, but forms a flat trigonal pyramid with a boron atom at its apex. Since the oxygen atoms at the two free corners of these BO_3 pyramids each belong to the neighbouring BO_4 tetrahedra, which, in their turn, behave in the structure just in the same manner as the tetrahedron initially chosen, the boron–oxygen linkage becomes endless, forming a rigid network.

Table 2. *Calculated and observed intensities of high-boracite*

Intensities were estimated visually in powder photographs (Cu $K\alpha$, $\lambda = 1{\cdot}45$ A.). For the Fourier synthesis, observed $hk0$ intensities were converted into numerical values on an arbitrary scale and were multiplied by the Lorentz, polarization and Debye–Waller ($B = 1{\cdot}0$) and other factors. The atomic f values used in calculating the structure amplitudes for the proposed structure were taken from the *International Tables* and were corrected for the heat motion, B being taken as 1·5 for chlorine and magnesium and 1·0 for boron and oxygen. $I_{calc.}$ values were obtained by the formula

$$I = k \frac{1+\cos^2 2\theta}{\sin^2 \theta \cos \theta} pF^2A,$$

where k is a constant, θ the Bragg angle, p the frequency factor and A the absorption coefficient.

Where lines are overlapped in the powder photograph, $F_{obs.}$ (for the Fourier synthesis) were assumed proportional to $F_{calc.}$ respectively. Phase angles for hkl are omitted.

hkl	$F_{calc.}$	$I_{calc.}$	$I_{obs.}$	$F_{obs.}$	hkl	$F_{calc.}$	$I_{calc.}$	$I_{obs.}$	$F_{obs.}$
200	85·5	40	*m*	90	10.2.0	45·6	20	*mw*	40
220	−24·0	4	*w*	35	862	53·5			
222	162·3	79	*ms*	—	951	37·1	6	—	—
400	344·2	219	*vs*	330	10.2.2	13·8	8	*w*	—
420	−190·6	230	*s*	160	666	89·0			
422	112·8	70	*m*	—	953	24·7	3	—	—
440	246·1	135	*ms*	180	10.4.0	−57·4	20	*w*	45
531	196·0	316	*vs*	—	864	49·0			
600	−34·0	3	—	50	10.4.2	47·3	12	*w*	—
442	20·4				880	151·7	31	*m*	165
620	59·6	14	*w*	70	971	32·7	6	—	—
622	158·1	93	*ms*	—	11.3.1	16·5			
444	335·0	123	*s*	—	10.4.4	80·0	29	*mw*	—
640	−114·3	44	*m*	100	882	64·3			
642	70·6	32	*m*	—	10.6.0	27·4	5	*w*	50
731	92·0	54	*m*	—	866	32·8			
800	215·8	35	*w*	120	973	35·8	7	—	—
820	−136·6	89	*m*	85	10.6.2	25·2	4	*w*	—
644	109·1				12.0.0	215·7	104	*m*	170
822	30·2	3	*w*	40	884	159·0			
660	16·0				11.5.1	35·4	7	—	—
751	53·1	16	—	—	12.2.0	−12·1	1	—	20
662	63·5	11	—	—	12.2.2	47·2	12	*w*	—
840	225·7	144	*ms*	150	10.6.4	29·5			
753	33·5	6	—	—	11.5.3	40·2	11	*w*	—
664	75·7	15	*w*	—	975	14·4			
931	54·0	15	—	—	12.4.0	124·0	48	*w*	80
844	236·0	142	*ms*	—					
10.0.0	54·1	4	—	75					
860	−30·9			30					

The flat BO_3 pyramid, which links three BO_4 tetrahedra in this way, in reality forms, with another oxygen atom, an acute oxygen pyramid, BO_3O, with a boron atom inside and near the basal plane. Four such BO_3O pyramids are joined with the common apex. Consequently, the boron–oxygen network may be defined broadly as a compact aggregate of BO_4 tetrahedra and BO_3O pyramids, holding the oxygen corners in common, and extending indefinitely throughout the structure.

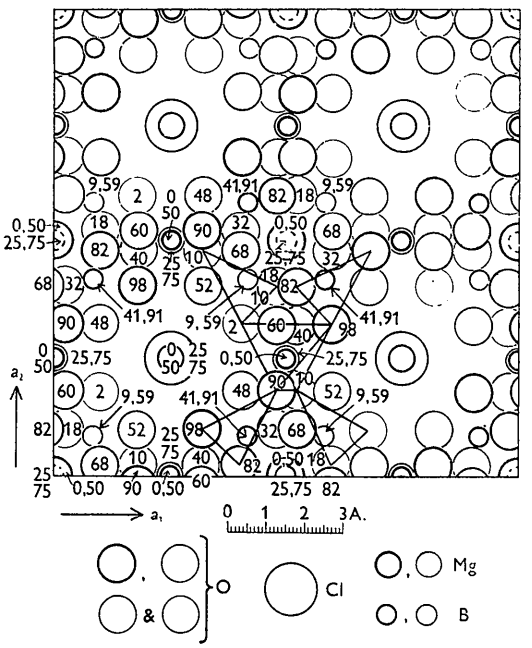

Fig. 1. Structure of high-boracite projected on (001). Numbers give the height of atoms from $(001)_0$, expressed as a percentage of the unit translation. A B_5O_{12} group (cf. Fig. 3) is traced.

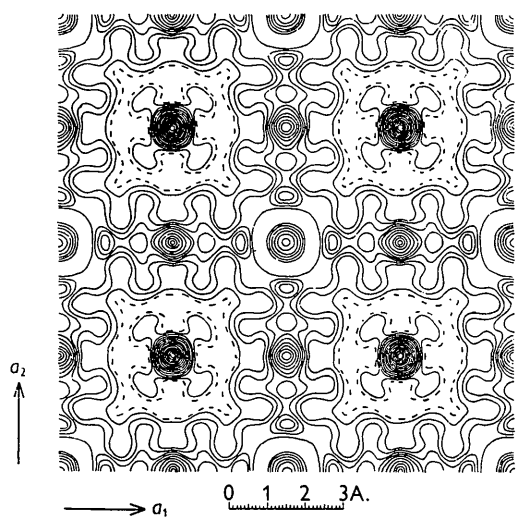

Fig. 2. Projection of electron density of high-boracite on (001). Contours at intervals of 4 e.A.$^{-2}$. The 4-electron levels are broken.

The magnesium and chlorine atoms occupy the space left vacant by the boron–oxygen framework. Each magnesium atom is surrounded octahedrally by four oxygen atoms (not exactly coplanar) and by two chlorine atoms. Each chlorine atom is held by six magnesium atoms. An oxygen atom is attached to two boron and one magnesium atoms or to four boron atoms.

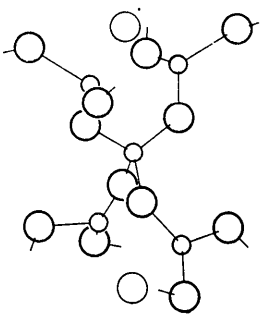

Fig. 3. The B_5O_{12} group singled out for convenience of description from the boron–oxygen network in the structure of high-boracite. Small circles represent boron atoms and large circles oxygen atoms. Oxygen atoms to be added to convert a flat BO_3 (trigonal) pyramid of the group into an acute BO_3O pyramid are shown by thin circles.

2. The structure of low-boracite

(i) *Experimental*

A series of Weissenberg–Buerger photographs (Mo $K\alpha$, $\lambda = 0{\cdot}71$ A.) was taken by rotating slips cut or ground from a 'single' crystal of low-boracite about the three crystallographic (morphological) axes. We have taken also several powder photographs (Cu $K\alpha$, $\lambda = 1{\cdot}54$ A.).

(ii) *Unit cell and space group*

The powder photograph of low-boracite permits an easy and perfect indexing on the basis of a cubic lattice with $a = 12{\cdot}07$ A. The rotation photographs, too, can be interpreted as of a cubic crystal in the first instance. However, low-boracite has hitherto been described as a mimetic twin composed of several individuals of varying shape and size (Friedel, 1904, p. 177; 1926, p. 274). The crystals we have examined were likewise made up of minute, optically diversely oriented laminae, and it was almost impossible to obtain a homogeneous slip free from twinning. Reflecting this, the Weissenberg photographs reveal infallibly that there are two or more identical sets of spots which can be discernibly ascribed to different individuals combined in the specimens. Further, the regular, though complex, alinement of these spots suggests that the component crystals are mutually oriented in a definite fashion.

In order to reduce these superimposed sets of spots to a single set and to deduce the mechanism of twinning, the method of the reciprocal lattice (Ito, 1938; 1950, p. 123) has been utilized. Taking advantage of the ability of the Weissenberg–Buerger photograph to represent the reciprocal lattice, we first derived the reciprocal-net planes from the photographs of various

levels, then piled them up in the order prescribed by experiment, and finally obtained a (three-dimensional) reciprocal lattice. We then resolved this composite lattice into three identical lattices and read off as the

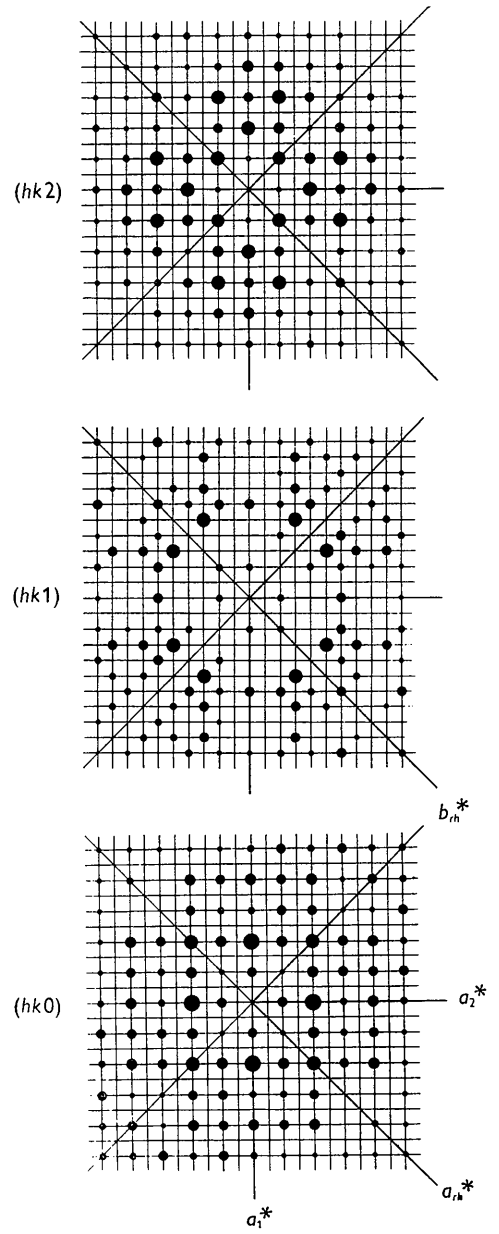

Fig. 4. The zero, first and second reciprocal-net planes (001)* of low-boracite. The size of spots is set approximately proportional to the intensity of reflexions observed. The original cubic and proper orthorhombic (reciprocal) axes are given in the figure, the third axes coinciding.

twinning operation a rotation of 120° about [111] (Friedel, 1904, p. 177; 1926, p. 472). The resulting lattice of low-boracite is shown, layer by layer, in Fig. 4, in which the size of spots are set approximately proportional to the intensity of reflexions observed in the photographs.

The intensity distribution on these diagrams indicates that, although the lattice might be perfectly described as cubic as far as the dimensions are concerned, it is in fact orthorhombic in symmetry, so that the axes must be changed accordingly. The transformation matrix from the cubic to orthorhombic (direct) axes is $\frac{1}{2}, \frac{1}{2}, 0/\frac{1}{2}, \bar{\frac{1}{2}}, 0/0, 0, 1$.

The unit cell now has

$$a = 8{\cdot}54, \quad b = 8{\cdot}54, \quad c = 12{\cdot}07\ \text{A.},$$

and contains four molecules of $ClMg_3B_7O_{13}$.

Taking into account pyroelectric and other properties, the space group of low-boracite has been determined to be either C_{2v}^5–*Pca*, C_{2v}^8–*Pba* or C_{2v}^9–*Pna*, *h*0*l* reflexions being present only when *h* is even, and 0*kl* reflexions only when *k* and *l* are even. Of these, the first is the most probable because it alone is a subgroup of T_d^5–$F\bar{4}3c$, the space group assigned to high-boracite. A choice, however, is deferred until we consider the arrangement of atoms.

(iii) *Analysis*

The inversion of boracite at 265° C. is reversible and accompanied by little or no change of lattice dimensions. Powder photographs of high- and low-boracite are practically identical. Upon close examination, however, we find in low-boracite a regularity of spectra, other than the space-group criteria, which markedly differentiates it from high-boracite and provides a clue to its

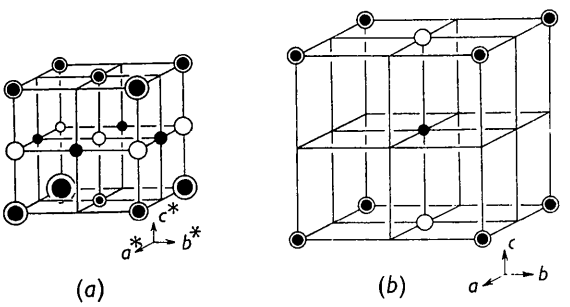

Fig. 5. The hybrid nature of the low-boracite lattice illustrated. (*a*) The reciprocal lattice as obtained from experiment. Open circles make up a base-centred and black circles a face-centred cell. (*b*) The (direct) lattice derived from, and corresponding to, (*a*). Open circles make up the base-centred and black circles the body-centred cell. Note that, whereas in the reciprocal lattice the unit volume of the face-centred cell is twice that of the base-centred cell superimposed, the volume of the corresponding body- and base-centred cells in the (direct) lattice is the same (Ito, 1950, p. 224).

structure. The rule is: *hkl* reflexions, if *l* is even, are present only when $h+k$ is even. This implies that, in terms of the reciprocal lattice, the cell is face- and base-centred at the same time (Fig. 5). Now the base-centred lattice is 'self-reciprocal', whereas the face-centred lattice is reciprocal to the body-centred lattice (Ito, 1950, p. 224). It may therefore be inferred that the (direct) lattice of low-boracite should have a mingled character of both base- and body-centred lattices,

some of the atoms being arranged on the body-centred and the remainder on the base-centred lattice. The structure as a whole, as required by the observed space-group criteria, is of course based on a simple lattice.

As we have seen, the structure of high-boracite is based on the face-centred lattice. If we describe this cubic structure in terms of the orthorhombic axes of low-boracite, a structure will result with all its constituent atoms arranged on a body-centred lattice. If we now leave the atoms of the boron–oxygen network in their original positions and displace the magnesium and chlorine atoms to such positions that they make up among themselves a base-centred lattice, we achieve an arrangement satisfying the requirement for a hybrid lattice.

Since, of the three possible space groups cited, C_{2v}^5–*Pca* alone is compatible with this structure, we assumed it to be the space group of low-boracite and proceeded with the determination of the atomic positions. The final parameters (Table 3) were determined by the two-dimensional Fourier syntheses on (001) and on (010), after the tentative structure derived along the lines discussed above had been verified by experimental data and refined considerably by trial and error. We omit the lengthy list of the observed and calculated F values and phase angles and give in Table 4 the reliability factors for the various categories of reflexions and also for all the reflexions observed. The relative F values (corrected for the polarization, Lorentz and temperature ($B=1{\cdot}0$) factors), obtained by the multiple photographic technique of Robertson, have been converted to absolute values by multiplying by a proportionality factor which makes the amplitude of the strongest observed reflexion (400) equal to the calculated value (180).

(iv) *Description of structure*

The structure of low-boracite, projection (001), is illustrated in Fig. 6; the corresponding Fourier map of electron density is shown in Fig. 7.

The structure is little different from that of high-boracite already described. It, too, consists of a three-dimensional unbroken boron–oxygen network with magnesium and chlorine atoms filling the interstices. The co-ordination of the magnesium and chlorine atoms is, however, different. Magnesium atoms in high-boracite are each fairly symmetrically surrounded by two chlorine and four oxygen atoms, but in low boracite they are more distant from one chlorine atom than from the other. Conversely, each chlorine atom in

Table 3. *Atomic co-ordinates of low-boracite*

The origin is placed at $\frac{1}{4}, \frac{1}{4}, 0$ with reference to that given in *International Tables*, the equivalent points being:
$x\,y,\,z;\quad \bar{x},\,y,\,\frac{1}{2}+z;\quad \frac{1}{2}+x,\,\frac{1}{2}-y,\,z;\quad \frac{1}{2}-x,\,\frac{1}{2}-y,\,\frac{1}{2}+z.$

Atom	No. of equivalent points in the cell	x/a	y/b	z/c
O_I	4	0	0	0
$O_{II(1)}$	4	0·082	−0·278	0·479
$O_{II(2)}$	4	0·159	0·201	0·402
$O_{II(3)}$	4	0·077	−0·119	0·320
$O_{II(4)}$	4	0·418	0·222	0·479
$O_{II(5)}$	4	0·341	−0·299	0·402
$O_{II(6)}$	4	0·423	0·381	0·320
$O_{II(7)}$	4	0·119	0·076	0·180
$O_{II(8)}$	4	0·201	−0·159	0·098
$O_{II(9)}$	4	0·222	−0·418	0·021
$O_{II(10)}$	4	0·381	−0·423	0·180
$O_{II(11)}$	4	0·299	0·341	0·098
$O_{II(12)}$	4	0·278	0·082	0·021
Cl	4	0·524	0	0·262
$Mg_{(1)}$	4	0·500	0	0·981
$Mg_{(2)}$	4	0·231	−0·269	0·250
$Mg_{(3)}$	4	0·231	0·269	0·250
$B_{I(1)}$	4	0·250	−0·250	0
$B_{I(2)}$	4	0	0	0·250
$B_{I(3)}$	4	−0·250	0·250	0
$B_{II(1)}$	4	0·500	0·330	0·415
$B_{II(2)}$	4	0·500	−0·330	0·415
$B_{II(3)}$	4	0·170	0	0·085
$B_{II(4)}$	4	0·170	0	−0·415

Table 4. *Reliability factors for the structure of low-boracite*

Reflexion	No. of observed reflexions	$R=\frac{\Sigma\lvert\lvert F_{obs.}\rvert-\lvert F_{calc.}\rvert\rvert}{\Sigma\lvert F_{obs.}\rvert}$
hkl	117	0·18
*hk*0*	66	0·19
*h*0*l*†	130	0·31
All reflexions observed	306	0·23

* *h*00 and 0*k*0 inclusive.

† *h*00 and 00*l* inclusive.

low-boracite is surrounded by six magnesium atoms, of which three are more separated from the central chlorine atom than the other three; in high-boracite the chlorine atoms are all equidistant from the neighbouring six magnesium atoms. Interatomic distances in high- and low-boracite are compared in Table 5.

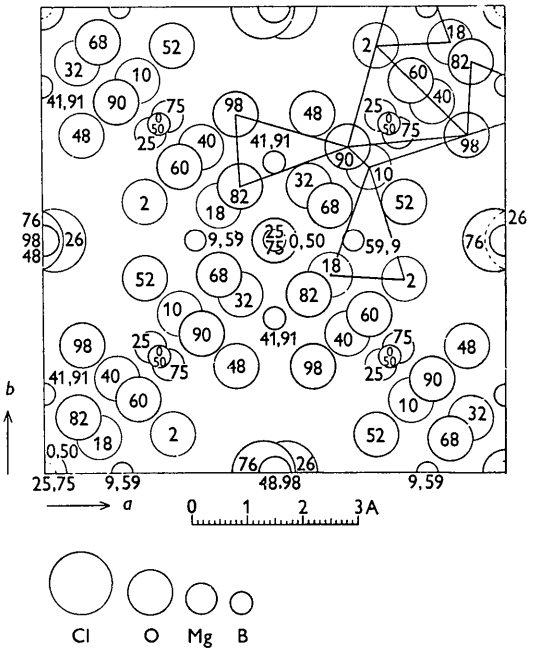

Fig. 6. Structure of low-boracite projected on (001). Numbers give the height of atoms from $(001)_0$, expressed as a percentage of the c translation. Part of a B_5O_{12} group (see Fig. 3) is traced to facilitate a comparison with the structure of high-boracite (see Fig. 1).

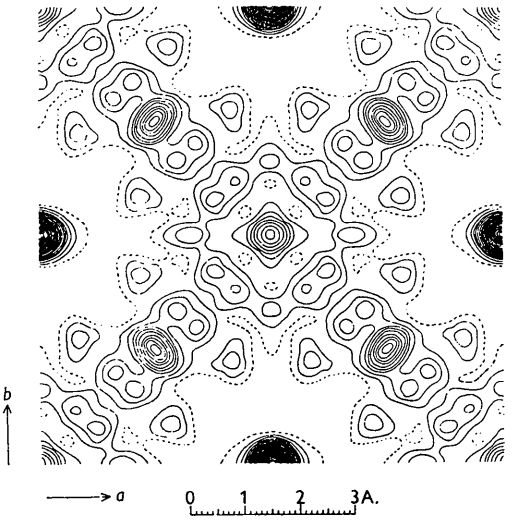

Fig. 7. Projection of electron density of low-boracite on (001). Contours at intervals of 5 e.A.$^{-2}$. The 5-electron levels are broken.

3. On the α–β inversion of boracite

We have worked out the structure of high-boracite by placing chlorine atoms in $(b)\frac{1}{4},\frac{1}{4},\frac{1}{4}$ positions with the point-symmetry T–23. Experiment, however, might

Table 5. *Interatomic distances in high- and low-boracite*

High-boracite			Low-boracite		
Atom	Neighbour	Distance (A.)	Atom	Neighbour	Distance (A.)
B_I	O_{II}	1·48	B_I	O_{II}	1·48
B_{II}	O_I	1·78	B_{II}	O_I	1·78
	O_{II}	1·39		O_{II}	1·39
Mg	O_{II}	2·04	Mg (1)	$O_{II(1)}$, $O_{II(4)}$	2·04
				$O_{II(9)}$, $O_{II(12)}$	2·06
			Mg (2)	$O_{II(3)}$, $O_{II(10)}$	2·04
				$O_{II(5)}$, $O_{II(8)}$	2·06
			Mg (3)	$O_{II(2)}$, $O_{II(11)}$	2·04
				$O_{II(6)}$, $O_{II(7)}$	2·06
	Cl	3·02	Mg (1, 2, 3)	Cl	2·65 or 3·40
O_I	O_{II}	2·50	O_I	O_{II}	2·50
O_{II}	O_{II} (tetrahedron)	2·42	O_{II}	O_{II} (tetrahedron)	2·42
	O_{II} (triangle)	2·37		O_{II} (triangle)	2·37
	O_{II} (octahedron)	2·90		O_{II} (octahedron)	2·90
Cl	O_{II}	3·44	Cl	$O_{II(1)}$	3·18 or 4·01
				$O_{II(4)}$	3·26 or 3·94
				$O_{II(9)}$	3·84 or 3·45
				$O_{II(12)}$	3·64 or 3·65

equally well be accounted for if, instead, we considered chlorine atoms as occupying a corner of the symmetry-bound tetrahedron around the same (*b*) points and swinging from one corner to the other. Although experimental data at our disposal are not sufficient to warrant a decision between these two versions, the Fourier projection of electron density of high-boracite (Fig. 2) is rather suggestive of the latter picture. The contour around chlorine atoms (overlapped by magnesium atoms in (100) projection) indicates conspicuous lumps just where chlorine atoms might be temporarily stationed in their swinging motion.

Should this be the real state of affairs, the α–β inversion would be adequately explained as due to the moving chlorine atoms simply coming to a standstill. At the transition temperature chlorine atoms may not shift from one definite position to another as we conceive ordinarily. It would be, indeed, difficult to understand why the inversion is accompanied by no observable effect on the lattice dimensions if a change in positions of certain atoms, and of their environment, had actually taken place.

References

Beckenkampf, J. (1933). *Hintze's Handbuch der Mineralogie.* Leipzig: Veit.

Cohn, W. M. (1928). *Z. Phys.* **50**, 124.

Friedel, G. (1904). *Étude sur les Groupements cristallins.* Saint-Étienne: Thomas.

Friedel, G. (1926). *Leçons de Cristallographie.* Paris: Berger-Levrault.

International Tables for the Determination of Crystal Structures (1935). Berlin: Borntraeger.

Ito, T. (1938). *Z. Krystallogr.* **100**, 437.

Ito, T. (1950). *X-ray Studies on Polymorphism.* Tokyo: Maruzen.

Mehmel, M. (1934*a*). *Z. Krystallogr.* **87**, 239.

Mehmel, M. (1934*b*). *Z. Krystallogr.* **88**, 1.

Sosman, R. B. (1924). *Properties of Silica.* New York: Chemical Catalog Co.

Acta Cryst. (1951). **4**, 316

The Crystal Structure of a Pentachlorocyclohexene, $C_6H_5Cl_5$

By R. A. Pasternak*

University College, London W.C. 1, *England*

(*Received* 26 *October* 1950)

The crystal structure of a pentachlorocyclohexene, prepared from the δ-isomer of $C_6H_6Cl_6$ by treatment with alkali, has been determined by Fourier projections, lines and selected sections. The position of the double bond has been fixed unambiguously. The steric course of elimination in the case of δ-$C_6H_6Cl_6$ has been established by this investigation.

Introduction

In the course of an extended investigation on the kinetics of olefin elimination from the isomers of hexachlorocyclohexane (Hughes, Ingold & Pasternak, unpublished; see also Cristol, 1945) intermediate products of the formula $C_6H_5Cl_5$ could be isolated in the case of the γ- and δ-isomers. Whereas the former was obtained as a viscous liquid, the latter crystallized from petrol ether. In order to clarify the steric course of elimination the X-ray analysis of this compound was undertaken.

Physical and X-ray data

$C_6H_5Cl_5$ (m.p. 69° C.) is very soluble in organic solvents. It crystallizes from light petrol ether in conglomerates of badly developed crystals, which are suitable neither for optical nor for X-ray measurements. Single crystals, however, occasionally appear at the wall of the crystallization flask as thin plates. Under the polarizing microscope they show a very high birefringence and are biaxial negative. The principal index, β, lies in the plane of the plate; the other two are inclined to it. From the X-ray measurements it was found that the crystals were monoclinic, the *b* axis being parallel to β. The face of the plate was chosen as (001).

Samples for the X-ray investigations were prepared by cutting such plates by a razor blade down to about equal dimensions (0·01–0·03 cm.). They were mounted in lithium borate tubes, as they deteriorated in the open air. Most of them were distorted and had to be rejected, but ultimately some fairly good crystals were found.

The unit-cell dimensions, determined from rotation and Weissenberg photographs, are

$$a=7\cdot54,\quad b=18\cdot2(8),\quad c=7\cdot01\text{ A.};\quad \beta=105\cdot(1)°.$$

Density (calculated for four molecules per unit cell), 1·811 g.cm.$^{-3}$; density (measured), 1·80 g.cm.$^{-3}$. Reflexions (0*k*0) and (*h*0*l*) are missing for *k* and *h* odd, respectively. The space group is therefore $P2_1/a$.

Weissenberg photographs were made of the (0*kl*)–(3*kl*), (*hk*0)–(*hk*3), (*h*0*l*)–(*h*6*l*) layer lines with Cu $K\alpha$ radiation, using the multiple-film technique. The relative intensities were estimated visually. They were corrected for Lorentz, polarization and inclination

* Present address: California Institute for Technology, Pasadena, California, U.S.A.